THE FIRST LASER GUIDE STAR ADAPTIVE OPTICS OBSERVATIONS OF THE GALACTIC CENTER: SGR A*'s INFRARED COLOR AND THE EXTENDED RED EMISSION IN ITS VICINITY

A. M. GHEZ,[1,2] S. D. HORNSTEIN,[1] J. R. LU,[1] A. BOUCHEZ,[3] D. LE MIGNANT,[3] M. A. VAN DAM,[3] P. WIZINOWICH,[3]
K. MATTHEWS,[4] M. MORRIS,[1] E. E. BECKLIN,[1] R. D. CAMPBELL,[3] J. C. Y. CHIN,[3] S. K. HARTMAN,[3]
E. M. JOHANSSON,[3] R. E. LAFON,[3] P. J. STOMSKI,[3] AND D. M. SUMMERS[3]

ABSTRACT

We present the first laser guide star adaptive optics (LGSAO) observations of the Galactic center. LGSAO has dramatically improved the quality and robustness with which high angular resolution infrared images of the Galactic center can be obtained with the Keck II 10 m telescope. Specifically, Strehl ratios of 0.7 and 0.3 at L' (3.8 μm) and K' (2.1 μm), respectively, are achieved in these LGSAO images; these are at least a factor of 2 higher and a factor of 4–5 more stable against atmospheric fluctuations than the Strehl ratios delivered thus far with the Keck natural guide star AO system on the Galactic center. Furthermore, these observations are the first that cover a large area ($76'' \times 76''$) surrounding the central black hole at diffraction-limited resolution for an 8–10 m class telescope. During our observations, the infrared counterpart to the central supermassive black hole, Sgr A*-IR, showed significant infrared intensity variations, with observed L' magnitudes ranging from 12.6 to 14.5 mag and a decrease in flux density of a factor of 2 over an 8 minute interval. The faintest end of our L' detections, 1.3 mJy (dereddened), is the lowest level of emission yet observed for this source by a factor of 3. No significant variation in the location of Sgr A*-IR is detected as a function of either wavelength or intensity. Previous claims of such positional variations are easily attributable to a nearby ($0''.09$ or 720 AU, projected), extended, very red source, which we suggest arises from a locally heated dust feature. Near a peak in its intensity, we obtained the first measurement of Sgr A*-IR's $K' - L'$ color; its $K' - L'$ of 3.0 ± 0.2 mag (observed) or 1.4 ± 0.2 (dereddened) corresponds to an intrinsic spectral index of $\alpha = -0.5 \pm 0.3$ for $F_\nu \propto \nu^\alpha$. This is significantly bluer than other recent infrared measurements from the literature, which suggest $\alpha = -4 \pm 1$. Because our measurement was taken at a time when Sgr A* was ~6 times brighter in the infrared than the other measurements, we posit that the spectral index of the emission arising from the vicinity of our Galaxy's central black hole may depend on the strength of the flare, with stronger flares giving rise to a higher fraction of high-energy electrons in the emitting region.

Subject headings: black hole physics — Galaxy: center — infrared: stars — techniques: high angular resolution

Online material: color figure

1. INTRODUCTION

High angular resolution infrared observations have had a large impact on our understanding of the center of the Milky Way. Application of speckle imaging techniques generated the first high angular resolution ($0''.05$–$0''.1$) images and demonstrated the existence of a supermassive ($\sim3.7 \times 10^6 \, M_\odot$) black hole through measurements of orbital motion in the plane of the sky for stars within the central few arcseconds of our Galaxy (e.g., Eckart & Genzel 1997; Ghez et al. 1998, 2000, 2003, 2005; Genzel et al. 2000; Eckart et al. 2002; Schödel et al. 2002, 2003). While these speckle imaging experiments resulted in the most convincing case of a supermassive black hole at the center of any normal-type galaxy, the application of this technique to the Galactic center has been limited primarily to proper motion measurements at a single wavelength. The advent of adaptive

optics (AO) systems that are based on natural guide stars (NGSs) allowed spectroscopy with sufficient angular and spectral resolution to detect weak absorption lines in individual stars orbiting in close proximity to the central black hole. These observations revealed that luminous stars located no more than 2000 AU from the central black hole are OB stars, which are thought to be less than 10 Myr old and which therefore raise the interesting question of how apparently young stars form in a region that is inhospitable to star formation (Ghez et al. 2003). These observations, in concert with the proper motion measurements, also provided a direct measurement of the distance to the Galactic center (Eisenhauer et al. 2003). NGSAO systems also increased the efficiency and depth of high angular resolution observations; this led to the discovery of an infrared counterpart to the central black hole, Sgr A*-IR (Genzel et al. 2003a; Ghez et al. 2004b), and permitted detailed studies of the stellar number density distribution, which suggested the existence of a central stellar cusp (Genzel et al. 2003b). While NGSAO has greatly enhanced the versatility of high angular resolution observations of the Galactic center, the quality of NGSAO observations degrades rapidly with both distance from the NGS and dimness of the NGS.

In this paper we present the first laser guide star adaptive optics (LGSAO) observations of the Galactic center. LGSAO has dramatically improved the quality and robustness with which high angular resolution images can be obtained with the Keck II 10 m telescope, revealing new features in the infrared emission coincident with and surrounding the central black hole, clear

[1] Division of Astronomy and Astrophysics, UCLA, Los Angeles, CA 90095-1547; ghez@astro.ucla.edu, seth@astro.ucla.edu, jlu@astro.ucla.edu, morris@astro.ucla.edu, becklin@astro.ucla.edu.
[2] Institute of Geophysics and Planetary Physics, UCLA, Los Angeles, CA 90095-1565.
[3] W. M. Keck Observatory, 65-1120 Mamalahoa Highway, Kamuela, HI 96743; abouchez@keck.hawaii.edu, davidl@keck.hawaii.edu, peterw@keck.hawaii.edu, rcampbell@keck.hawaii.edu, jchin@keck.hawaii.edu, mvandam@keck.hawaii.edu, shartman@keck.hawaii.edu, erikj@keck.hawaii.edu, rlafon@keck.hawaii.edu, pstomski@keck.hawaii.edu, dsummers@keck.hawaii.edu.
[4] Caltech Optical Observatories, California Institute of Technology, MS 320-47, Pasadena, CA 91125; kym@caltech.edu.

short-timescale variations in the infrared emission arising from just outside the black hole, and the first measurement of Sgr A*-IR's $K' - L'$ color. Furthermore, these observations are the first that can cover a large area surrounding the central black hole at diffraction-limited resolution. These measurements represent an exciting next step in our understanding of the central black hole and its surrounding, as well as in our technical ability to obtain high angular resolution data.

2. OBSERVATIONS

Images of the Galactic center were obtained on 2004 July 26 (UT) with the Keck II 10 m telescope using the new facility LGSAO system (P. Wizinowich et al. 2005, in preparation; M. van Dam et al. 2005, in preparation) and the near-infrared camera, NIRC2 (K. Matthews 2005, in preparation). During these observations, an artificial guide star was generated with a pulsed dye laser, which was tuned to the Na D atomic transition (589 nm) and which was run at 14 W output power. At the beginning of the night, the size of the LGS, imaged at zenith with the whole telescope pupil, was measured to be $1\rlap.{''}3 \times 2\rlap.{''}1$, elongated due to the finite thickness of the sodium layer. The size of the LGS across the wavefront sensor varied from $1\rlap.{''}2 \times 1\rlap.{''}4$ close to the location of the LGS launch telescope to $1\rlap.{''}5 \times 3\rlap.{''}1$ for the spots farthest from the launch telescope. Although the intrinsic LGS spot size increases with increasing air mass (AM) due to additional turbulence on its upward and downward trajectory, the spot elongation decreases, since the LGS is at a larger distance from the telescope. Over the course of our observations, the LGS brightness was equivalent to a V magnitude of 11.4 star, and it varied by only 5% (1 σ). For all the observations reported here, the LGS's position was always locked to the center of the NIRC2 field of view.

While observations of the artificial guide star provide the necessary information to correct most of the important atmospheric aberrations, it does not provide information on the tip-tilt term, which, for these observations, was obtained from visible observations of USNO 0600-28577051 ($R = 13.7$ mag and $\Delta r_{\mathrm{SgrA}^*} = 19''$). The science instrument houses a 1024×1024 InSb array, which has pixel scales of 9.93 and 39.9 mas pixel^{-1} and corresponding fields of view of $10\rlap.{''}2 \times 10\rlap.{''}2$ and $40\rlap.{''}8 \times 40\rlap.{''}8$, respectively. All observations were made using correlated double-sampling readout of the array, which produced an rms readout noise of 77 electrons. With the LGSAO/NIRC2 setup, two sets of eight 30 s narrow-field images, each composed of 120 co-added 0.25 s exposures, were obtained through the L' ($\lambda_o = 3.78$ μm, $\Delta\lambda = 0.70$ μm) photometric bandpass; each set of eight images was composed of four pairs of images centered at the corners of a $0\rlap.{''}5 \times 0\rlap.{''}5$ box. Twelve additional 9 s K' ($\lambda = 2.12$ μm, $\Delta\lambda = 0.35$ μm) narrow-field images, each composed of 50 co-added 0.181 s exposures, were collected. In the wide field-of-view mode, two sets of five 25 s (100 co-added 0.25 exposures) narrow bandpass filter (set 1 [He I filter]: $\lambda_o = 2.06$ μm, $\Delta\lambda = 0.03$ μm; set 2 [narrowband continuum filter]: $\lambda_o = 2.27$ μm, $\Delta\lambda = 0.03$ μm) images, dithered by 18'' to create a $76'' \times 76''$ field of view, were also obtained. A similar sequence on a relatively dark portion of the sky was observed both before and after the Galactic center observations to measure the background emission.

The operational efficiency of the LGSAO system was quite high. Before these observations could begin, roughly 5 minutes were required to acquire the tip-tilt star and propagate the laser. After this initial set-up time, the only other overhead introduced by the LGSAO system was an additional ~20 s with each dither to move the laser to the new field center. P. Wizinowich et al.

(2005, in preparation) provide further details on the science observing efficiency for the LGSAO system in all its possible observing modes.

During these measurements, the uncorrected 2 μm seeing disk size for observations of the Galactic center was $\sim0\rlap.{''}5$, which is close to the median value of $0\rlap.{''}4$ for the Keck telescopes. On-axis K' LGSAO observations of the tip-tilt star, which were taken just before the observations centered on Sgr A* at an AM of 1.53, yielded a point-spread function (PSF) with a Strehl ratio of 0.422 and a FWHM of 52.3 mas. Compared to the LGSAO performance for observations centered on Sgr A*, which yield an average K' Strehl ratio of 0.31 (see § 4 for detailed description of LGSAO performance), this implies an atmospheric isokinetic angle[5] of $34''$ $(1.53/AM)^{1.5}$ for these observations and $64''$ for observations at zenith.

3. DATA ANALYSIS

The standard image reduction steps of background subtraction, flat-fielding, bad pixel repair, and optical distortion correction were carried out on each image. Since the background in the L' images is dominated by the thermal emission from the AO system, the best background subtraction was achieved by subtracting from each image the average of sky images that were taken with as similar a rotator angle as possible.

The optical distortion corrections applied were taken from the NIRC2 preship review results[6] and are relatively small for the narrow field-of-view camera. The preship review results do not adequately describe the optical distortions in the wide field-of-view camera. We therefore restrict our analysis of the wide field data set to the small region around Sgr A*-IR and will report the results of our search for stars with He I line features, which are more sensitive to these field variations, elsewhere (J. R. Lu et al. 2005, in preparation).

Point sources were identified and characterized in both the individual images and in an average of all the images by running them through the PSF fitting program, StarFinder (Diolaiti et al. 2000). This generated an estimate of each image's PSF based on the several bright point sources (IRS 16C, 16NW, 29N, 16NE, and 33E for the K' images and IRS 16C, 16NW, and 29NE in the L' images) and relative flux densities for all sources that were identified. Using the apparent magnitudes measured by Blum et al. 1996 at K and S. A. Wright et al. (2005, in preparation) at L' for IRS 16NE ($K = 9.00$, $L' = 7.37$ mag), IRS 16NW ($K = 10.03$, $L' = 8.43$ mag), and IRS 16C ($K = 9.83$, $L' = 8.14$ mag), we derived apparent magnitudes for all the sources detected with StarFinder and estimated the uncertainties in the calibration to be $\sim4\%$ and 5% for the K' and L' observations, respectively.[7] The apparent magnitudes were dereddened assuming a visual extinction of 29 ± 1 mag from S. A. Wright et al. (2005, in preparation) and an extinction law derived by Moneti et al. (2001), and then converted to flux densities with zero points from Tokunaga 2000 (see the footnotes in Table 1 for values).

Extra steps were taken with StarFinder to ensure that Sgr A*-IR, which is located in a very crowded region, was accurately measured in the individual short-exposure frames. First, StarFinder

---

[5] The isokinetic angle, θ_{TA}, is the characteristic angular offset at which the RMS wavefront error due to tilt decorrelation (σ_{TA}) is 1 rad [$\sigma_{\mathrm{TA}}^2 = (\theta/\theta_{\mathrm{TA}})^2$], where θ is the distance from the tip-tilt star; Hardy 1998].

[6] See http://alamoana.keck.hawaii.edu/inst/nirc2.

[7] The formal uncertainty for the K' absolute magnitudes is only 2%, but we increase it to 4% to accommodate the differences between the K and K' filters. Nonetheless, our final reported uncertainties are dominated by the relative flux measurements as opposed to this absolute calibration uncertainty.

TABLE 1
Summary of 2004 July 26 (UT) LGSAO Time-resolved Observations of Sgr A*-IR

File	Time (UTC)	T_{exp} (s)	σ_{wf}[a] (nm)	FWHM (mas) K'	FWHM (mas) L'	Strehl Ratio K'	Strehl Ratio L'	K' Brightness Observed Mag.	K' Brightness F_ν (mJy)[b,c]	L' Brightness Observed Mag.	L' Brightness F_ν (mJy)[b,c]
77..........	08:18:50	9	344	66	...	0.36	...	15.85 ± 0.22	5.9 ± 1.2	...	...
78..........	08:19:58	9	340	63	...	0.36	...	16.10 ± 0.32	4.7 ± 1.4	...	...
79..........	08:21:34	9	346	62	...	0.35	...	15.50 ± 0.16	8.1 ± 1.2	...	...
80..........	08:21:59	9	343	62	...	0.36	...	15.64 ± 0.18	7.1 ± 1.2	...	...
81..........	08:22:53	9	427	83	...	0.20	...	15.23 ± 0.15	10.4 ± 1.4	...	...
83..........	08:24:04	9	387	73	...	0.27	...	>15.08[d]	<12.0	...	...
84..........	08:24:30	9	346	62	...	0.35	...	15.57 ± 0.17	7.6 ± 1.2	...	...
85..........	08:25:14	9	382	72	...	0.29	...	15.77 ± 0.20	6.3 ± 1.2	...	...
86..........	08:25:40	9	328	59	...	0.39	...	15.63 ± 0.18	7.2 ± 1.2	...	...
87..........	08:27:04	30	378	...	81.1	...	0.67	...	...	12.58 ± 0.09	9.74 ± 0.79
88..........	08:28:02	30	378	...	81.9	...	0.67	...	...	12.64 ± 0.08	9.21 ± 0.68
89..........	08:29:31	30	329	...	80.6	...	0.74	...	...	12.81 ± 0.10	7.88 ± 0.71
90..........	08:30:29	30	316	...	80.3	...	0.76	...	...	12.90 ± 0.11	7.25 ± 0.76
91..........	08:31:46	30	337	...	80.4	...	0.73	...	...	12.89 ± 0.12	7.32 ± 0.78
92..........	08:32:45	30	347	...	80.6	...	0.72	...	...	12.84 ± 0.10	7.66 ± 0.72
93..........	08:34:02	30	360	...	80.8	...	0.70	...	...	12.99 ± 0.12	6.67 ± 0.74
94..........	08:35:00	30	370	...	81.8	...	0.68	...	...	13.19 ± 0.14	5.55 ± 0.71
95..........	08:39:19	25	...	...	...	...	...	>16.66[d,e]	<2.8	...	...
104..........	08:49:42	25	...	...	...	...	...	>16.31[d,e]	<3.5	...	...
113-4	09:00:19	18	371	65.2	...	0.30	...	>16.00[d]	<5.1	...	...
115..........	09:02:10	30	404	...	82.7	...	0.64	...	...	14.31 ± 0.19	1.98 ± 0.35
116..........	09:03:08	30	403	...	81.8	...	0.64	...	...	14.54 ± 0.21	1.60 ± 0.30
117..........	09:04:22	30	399	...	81.6	...	0.64	...	...	14.52 ± 0.20	1.63 ± 0.30
118..........	09:05:28	30	405	...	82.0	...	0.64	...	...	14.56 ± 0.21	1.57 ± 0.30
119..........	09:06:45	30	394	...	80.4	...	0.65	...	...	14.56 ± 0.21	1.57 ± 0.30
120..........	09:07:44	30	419	...	82.0	...	0.62	...	...	14.78 ± 0.26	1.28 ± 0.30
121..........	09:09:04	30	372	...	81.3	...	0.68	...	...	14.74 ± 0.25	1.33 ± 0.30
122..........	09:10:02	30	377	...	82.2	...	0.67	...	...	14.73 ± 0.25	1.34 ± 0.30

[a] σ_{wf} is the rms wavefront error

[b] The values given for flux densities are dereddened flux densities and derived from the apparent magnitudes with the following assumptions: (1) a visual extinction of 29 ± 1 mag from S. A. Wright et al. (2005, in preparation) and an extinction law derived by Moneti et al. (2001; $A_{2.2\mu m}/A_V = 0.1108$; $A_{3.8\mu m}/A_V = 0.0540$), which gives a K' extinction of 3.21 mag and an L' extinction of 1.57 mag, and (2) zero points (i.e., the flux density of a 0 mag star) for the K' and L' magnitude scales of 667 and 248 Jy, respectively (Tokunaga 2000).

[c] The uncertainties in the dereddened flux densities do not explicitly include the dereddening uncertainties, which are ~5% at K' and ~11% at L'. For our measurements, these are only significant at L'.

[d] 3 σ limits

[e] These values are from the data sets obtained with the wide-field camera (and hence we do not attempt to report the PSF characteristics) and narrow band-pass filters.

was run using a detection threshold of 0.6 for the correlation between a source and the PSF. Second, StarFinder was run in a mode in which it fit only sources from an input list. Our list included all sources detected from the first step along with any source within 0″.15 of the dynamical center that was detected in the average map at that wavelength, but was missed in the first step for that individual short exposure.[8] Since StarFinder's PSF fitting routine is very sensitive to local confusion, these added sources, if overlooked, can affect the resulting photometry. Since frame 82 had an anomalously poor-quality PSF and StarFinder failed to identify any of the sources within 0″.1 of Sgr A*-IR in this first step, it was dropped from any further analysis. The second step recovered all the missing detections of these central sources except for Sgr A*-IR in three K' maps and S0-20 in one L' map. The consecutive images 113 and 114 with no detections of Sgr A*-IR were averaged together and analyzed as described above but still led to a nondetection of Sgr A*-IR.

[8] The following sources within the central 0″.15 were missed in the first step: Sgr A*-IR in five K' and eight L' maps, S0-17 in one K' and four L' maps, and S0-20 in one K' and four L' maps.

Uncertainties in Sgr A*-IR's photometry were estimated from the flux density fluctuations between the maps for stars that are detected in at least 75% of the maps. Since the stars are not variable on the timescale of this experiment and the image quality is fairly constant across the maps, the rms of these stars' flux densities provides an estimate of the measurement uncertainty as a function of flux density. We therefore set the uncertainty in a given Sgr A*-IR flux density measurement equal to the average rms of stars whose flux density differs by no more than 1 mJy from that measurement of Sgr A*-IR. Between 10 and 75 stars contribute to most of these uncertainty estimates, depending on the brightness of Sgr A*-IR.

For the two K' maps without detections of Sgr A*-IR (image 83 and the average of images 113 and 114), upper limits on Sgr A*-IR's flux density are derived from aperture photometry. In order to remove the effects of nearby stars in such a crowded region, we subtracted, from the original map, the model created by StarFinder of all the detected point sources, with the exception of two sources at $r > 0″.1$ that served as photometric reference sources (S0-19 and S0-8; see Table 2). Aperture photometry was then conducted on this difference map, using an aperture radius of ~0″.06 and a surrounding sky annulus of width ~0″.03, at the

TABLE 2
Summary of Key Detections in the Average LGSAO Maps from 2004 July 26 (UT)

Name	Other Name[a]	r (arcsec)	$\Delta\alpha_{\text{dyn. cent.}}$ (arcsec)	$\Delta\delta_{\text{dyn. cent.}}$ (arcsec)	K' (mag)	L' (mag)
Sources within 0″.15 of Dynamical Center of the Galaxy						
Sgr A*-IR...............	...	0.00	0.00	0.00	15.99 ± 0.06	13.39 ± 0.09
Extended Red............	...	0.10	-0.07	-0.07	<16.2	13.64 ± 0.15
Emission						
S0-17......................	...	0.10	0.03	-0.10	15.52 ± 0.06	13.93 ± 0.12
S0-2........................	S2	0.12	0.03	0.12	14.17 ± 0.03	12.78 ± 0.03
S0-20......................	S13	0.14	-0.11	0.08	15.74 ± 0.20	14.18 ± 0.07
Sources Used to Establish Detection Limits						
S0-19......................	S12	0.32	-0.06	0.31	15.40 ± 0.08	13.92 ± 0.03
S0-8........................	ID14	0.37	-0.28	0.24	15.68 ± 0.07	14.01 ± 0.05

[a] Other names from Schödel et al. (2003).

locations of Sgr A*-IR, the reference sources, and a few background locations near Sgr A*-IR. These were combined to generate 3 σ detection limits. A similar analysis was carried out on the two wide-field maps that contained Sgr A*-IR.

4. LGSAO PERFORMANCE

The LGSAO system has dramatically improved the versatility, image quality, and robustness of adaptive optics observations of the Galactic center. Based on the PSFs estimated from StarFinder (see § 3), the images all have consistently high Strehl ratios, 0.68 ± 0.04 for the L' (3.8 μm)–band images and 0.31 ± 0.06 for the K' (2.1 μm)–band images, as well as PSF full width at half maxima (FWHMs) that are also all consistently very nearly diffraction-limited; at L' the FWHM is 80.6 ± 0.7 mas and at K' the FWHM is 63 ± 8 mas. Using the extended Maréchal approximation that $S = e^{-(2\pi\sigma_{\text{wf}}/\lambda)^2}$, where S is the Strehl ratio, σ_{wf} is the rms wavefront error, and λ is the observing wavelength, we find an average rms wavefront error of 371 ± 30 nm for these observations. Compared to the Keck natural guide star adaptive optics (NGSAO) system, the LGSAO system can observe the Galactic center under much poorer atmospheric conditions and delivers L' images that have, on average, a factor of 2 higher Strehl ratios and are a factor of 4–6 more stable. Specifically, during our best L' NGSAO nights (2002–2004), images have Strehl ratios of 0.33 ± 0.06 and PSF FWHM of 93 ± 5, or equivalently σ_{wf} of 620 ± 50 nm (see Ghez et al. 2004a, 2004b; S. D. Hornstein
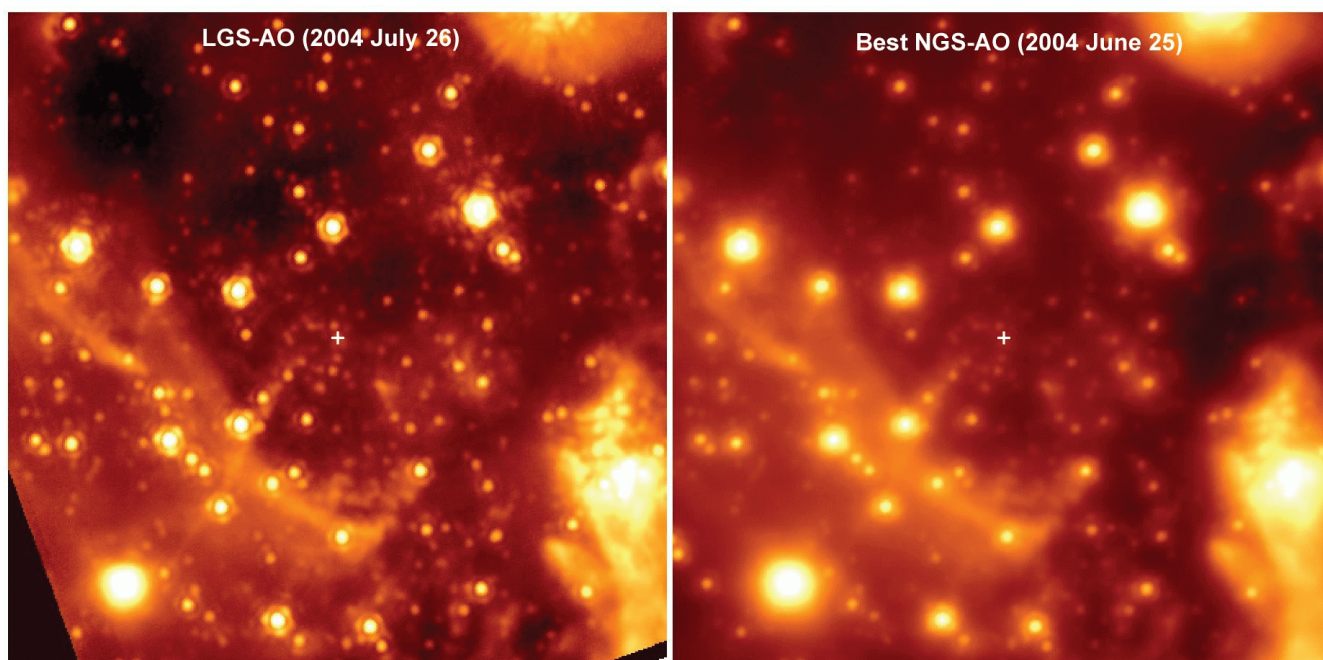

Fig. 1.—Comparison of the first LGSAO image (*left*) and the best NGSAO image (*right*) taken with the Keck II 10 m telescope (2002–2004) in the L' (3.8 μm) photometric bandpass of the central 7″.5 × 7″.5 of our Galaxy. In both images, the cross denotes the location of the central supermassive black hole, and the orientation is north is up and east to the left. The LGSAO image has a Strehl ratio that is a factor of 2 higher than that obtained in the NGSAO image; furthermore, the LGSAO image resulted from an exposure time of only 8 minutes, a factor of ~20 less than the comparison NGSAO image. The LGSAO system has therefore dramatically improved the image quality that can be obtained on the Galactic center with the Keck telescope.
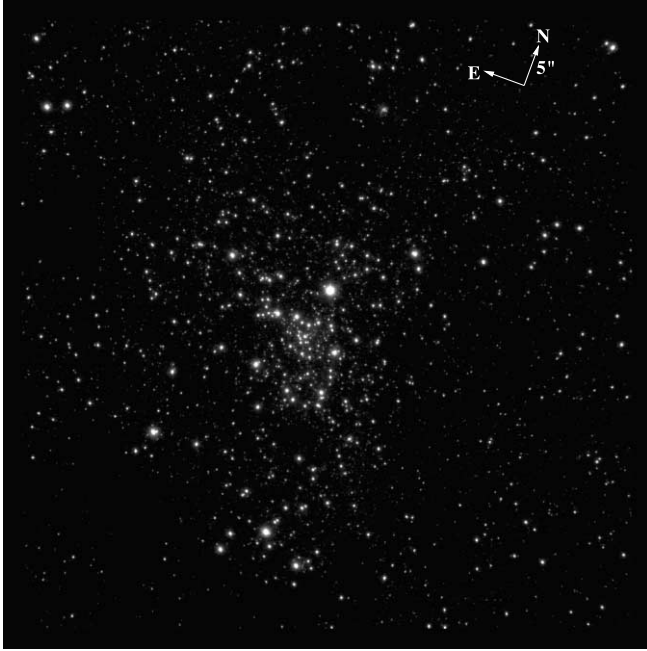
FIG. 2.—A $76'' \times 76''$ diffraction-limited 2 μm mosaic of the Galactic center obtained with five pointings of the LGSAO system. This is the widest near-infrared field imaged yet at this angular resolution. [*See the electronic edition of the Journal for a color version of this figure.*]

et al. 2005, in preparation). This improvement is depicted in Figure 1, which compares the average of all our L' LGSAO images to the best NGSAO L' image that we obtained at the Keck telescope between 2002 and 2004; the improvement stems primarily from having a much brighter, by about 2 mag, on-axis source to correct for the non–tip/tilt atmospheric aberrations with the LGSAO system, compared to the faint ($R = 13.2$ mag) off-axis ($30''$) star used for the NGSAO observations. The LGSAO image is the highest quality L' image obtained thus far of the center of our Galaxy. Somewhat better K' performance has been obtained with the VLT's NGSAO system, since it has an infrared wave-front sensor to take advantage of the bright, very nearby, infrared source IRS7 ($K = 6.4$ mag) and the Galactic center passes directly overhead (vs. a $50°$ zenith angle from Hawaii). However, this is only possible within the isoplanatic angle ($\sim 20''$ at 2 μm) of this source, since no other comparably bright infrared source exists in this region. Figure 2 shows the remarkably large field coverage that is now possible with the LGSAO system. This $76'' \times 76''$ region is the largest area imaged at the diffraction limit of a $8-10$ m telescope by a factor of 4 and has a much more uniform PSF over comparable areas. This approach is limited only by the isokinetic angle ($\sim 40''-75''$ at 2 μm), which is much larger than the isoplanatic angle, and by the availability of tip-tilt stars, which need not be as bright as the NGSs necessary to correct all the aberrations, and which are therefore much more plentiful.

5. RESULTS

The improved image quality greatly facilitates detailed study of the infrared emission arising in the crowded region in the vicinity of our Galaxy's central black hole. Within a radius of $0''\!.15$ of the dynamical center of our Galaxy, there are three known proper motion sources (S0-2, S0-17, and S0-20; Ghez et al. 2005), all of which are detected in both the K' and L' LGSAO images (see Table 2 and Fig. 3). In addition, the L' LGSAO image reveals a new source ($L' \sim 13.3$ mag), whose photocenter is
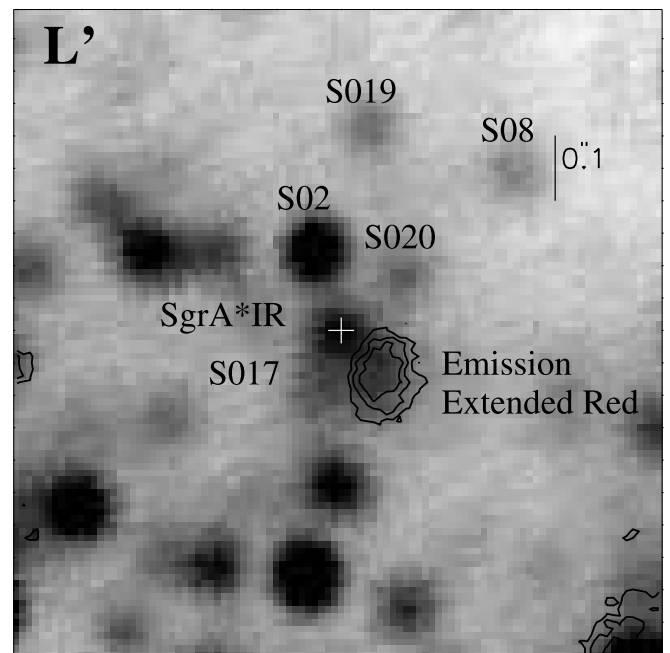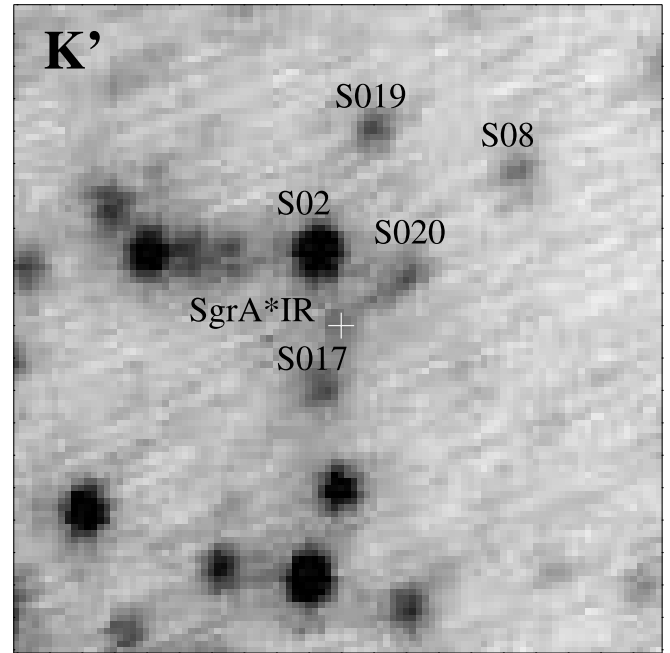

FIG. 3.—Central $1'' \times 1''$ region of the average of all the K' (*top*) and L' (*bottom*) LGSAO images. The position of Sgr A*-IR is marked with a white cross, and the labeled sources are those that are either within $0''\!.15$ of the dynamical center (extended red emission, S0-17, S0-2, and S0-20) or that were used to establish upper limits for detection (S0-19 and S0-8). The contour image is what remains after subtracting out all identified point sources, leaving primarily just the emission from the extended source. North is up and east is to the left.

located $0''\!.094$ southwest from Sgr A*-IR (see Fig. 3, *bottom*). This source, which was originally reported by Ghez et al. (2004b) and has since been independently reported by Clénet et al. (2005; labeled Sgr A*-f), can be equally well modeled as two roughly equal point sources separated by $0''\!.057$ or as a two-dimensional Gaussian that has a major axis of 120 mas (corresponding to an intrinsic size of ~ 80 mas). No source is detected at this location in the K' LGSAO image down to ~ 16.1 mag (2 σ), which implies that its ($K' - L'$) must be redder than 2.8 mag (observed)
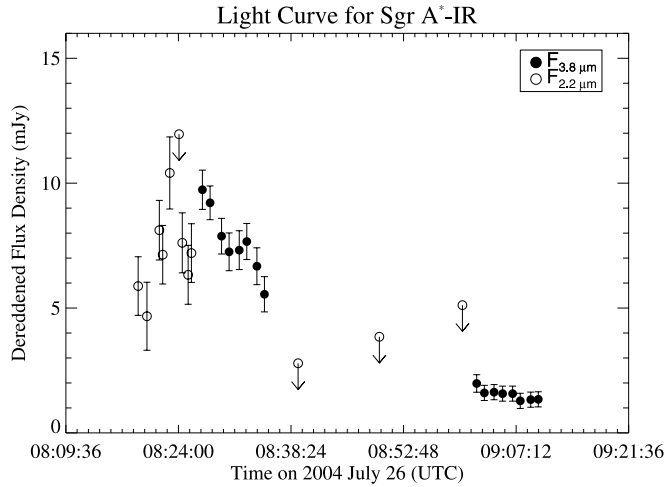
FIG. 4.—Light curve for Sgr A*-IR. The near simultaneity (within 1 minute) of the K' and L' measurements at ∼8:26 (UT) provides the first measurement of Sgr A*-IR's $K' - L'$ color. Significant flux density variations are also detected both within the K' (*open circles*) and L' (*filled circles*) measurements. The emission from Sgr A*-IR is observed to increase, peak, and then decrease by a factor of 2 in 8 minutes. Another ∼30 minutes later it is observed to have a flux density of only 1.3 mJy at 3.8 μm. This is the lowest level Sgr A*-IR has ever been detected by a factor of 3, suggesting that no true steady state level has yet been observed.

or 1.2 mag (dereddened). Combining the photocenter of this LGSAO detection with the photocenter detections of this source in our earlier NGSAO maps (Ghez et al. 2004b [2002 May 31 and 2003 June 10, 16–17]; S. D. Hornstein et al. 2005, in preparation [2004 June 25–28 and 2004 July 6–7]), which do not spatially resolve the source, we find its proper motion to be statistically consistent with zero to within 2 σ (9.6 ± 4.1 mas yr^{-1}).

In spite of the stellar crowding, Sgr A*-IR is also clearly detected in both the average K' and L' images, as well as in the majority of the individual L' and K' images (see Table 1 and Figs. 3 and 4). At the beginning of our observations, Sgr A*-IR at K' appears to brighten and reach a peak of $K'_{obs} \sim 15.5$. At the end of the K' sequence, Sgr A* has a K'_{obs} magnitude of 15.6 ± 0.2 or, equivalently, a dereddened flux density of 7 ± 1 mJy. After a time gap of ∼1 minute, its observed L' magnitude is 12.58 ± 0.09 ($F_{3.8\mu m, dered} = 9.7 \pm 0.8$ mJy). This provides an estimate of the color of Sgr A* of $(K' - L')$obs = 3.0 ± 0.2 or $(K' - L')$dereddened = 1.4 ± 0.2. Over the course of only 8 minutes, its flux density decreases by a factor of 2 and, another 27 minutes later, Sgr A* is a factor of 3 fainter still, or 1.3 mJy (dereddened), in the L' photometric bandpass. This is the faintest that Sgr A*-IR has ever been detected at L', by a factor of 3. From the average images, we find that Sgr A*-IR's positional offsets from the Galaxy's dynamical center are statistically consistent with zero at both K' and L' ([$\Delta_{R.A.,K'} = -2 \pm 4$ mas, $\Delta_{decl.,K'} = 0 \pm 3$ mas] and [$\Delta_{R.A.,L'} = -4 \pm 2$ mas, $\Delta_{decl.,L'} = -7 \pm 3$ mas], using the Ghez et al. [2005] determination of the dynamical center). From the individual images, there is no evidence for variation in the location of Sgr A*-IR as a function intensity; previous claims of such positional variations from Clénet et al. (2005) at L' are easily attributable to the nearby extended, very red source discussed above.

Since both the photometric and astrometric measurements were made with a PSF-fitting routine and since all the known neighboring sources as well as a background, which is allowed to have low spatial frequency structure, are part of the model, our reported values should be free of bias from the surrounding stellar population and background emission.

6. DISCUSSION

6.1. Extended Red Emission in the Vicinity of Sgr A*

There are several possible explanations for the extended red source located 90 mas southwest of Sgr A*. First, one might consider that it consists of multiple red stars that are blended in the image. However, we expect the old stellar population to be centered on Sgr A*, so if this were the explanation, the displacement would have to be due to the chance placement of a relatively small number of objects, presumably giants. However, even giants are not as red as the extended red emission, unless they are subject to additional extinction beyond that suffered by Sgr A*. This would then have to correspond to an unlikely placement of multiple giants remarkably close in projection to Sgr A*, yet located in the background behind additional extinction. A second possibility is that this emission is from an off-center region within an accretion disk around Sgr A*. Off-center brightening in an accretion disk has been predicted by Nayakshin et al. (2004) as a response to the passage of stars through the accretion disk, but this mechanism gives rise to an unresolved source, rather than to the observed, extended emission, so one would have to posit multiple recent star-disk passages in this particular region, which is also rather unlikely.

The third explanation is that the extended red source is attributable to thermal emission from a dust cloud. Indeed, there is a dust feature projected near Sgr A* in this direction, as can be seen in mid-IR images (Stolovy et al. 1996). It is tempting to hypothesize that this feature lies close to Sgr A* and that energy from Sgr A* and its immediate entourage of early-type stars heats the dust, giving rise to a temperature gradient that declines away from Sgr A*. However, if the extended dust feature is close enough to Sgr A* to be heated by it, it is problematic that it has not already been sheared by the tidal interaction into a ring around Sgr A*. Furthermore, for an intact object, we would expect a displacement on the order of 60 mas yr^{-1}—far larger than our limit of ∼10 mas yr^{-1}—if the distance of the extended red feature from Sgr A* were comparable to its projected distance of 94 mas. It is therefore quite likely that the extended red dust feature is projected along the line of sight toward Sgr A* and that it is heated by an embedded or a nearby star.

Only a small amount of dust is required to generate the observed emission. The 3.8 μm opacity of the dust cloud must be quite small, given its size and surface brightness: $\tau(T_d) = 10^{-6} \times [\exp(3787/1200 K) - 1]/[\exp(3787/T_d) - 1]$. Here the dust temperature, T_d, is referenced to its upper limit of 1200 K, derived from the dereddened limit on the $K' - L'$ color, and assuming an emissivity dependence $Q_\lambda \propto \lambda^{-1}$. With these assumptions, the bolometric luminosity of the source can be crudely estimated: $L = 1.2 L_\odot (T_d/1200)^5 \tau(T_d)/\tau(1200 K)$. Assuming further that the source depth is equal to its width on the sky, and that the gas-to-dust ratio is 100, we find a total source mass equal to $1.3 \times 10^{-10} M_\odot \tau(T_d)/\tau(1200 K)$, clearly a very modest clump.

6.2. Infrared Color of Sgr A*

The radiative emission emerging from the vicinity of our Galaxy's supermassive black hole has puzzled modelers for three decades. Its total luminosity is only 10^{36} ergs s^{-1}, or 10^{-9} of the Eddington luminosity for a $3.7 \times 10^6 M_\odot$ black hole, most of which is emitted at radio wavelengths. To account for the low luminosity, current models rely on radiative inefficiencies in either, or some combination of, an accretion flow or an outflow (see, e.g., review by Melia & Falcke 2001). Further complicating the picture, recent observations have revealed X-ray and

infrared emission, which both show significant variability at time-scales as short as tens of minutes (Baganoff et al. 2001; Goldwurm et al. 2003; Porquet et al. 2005; Genzel et al. 2003a; Ghez et al. 2004b; Eckart et al. 2004). While there is still considerable debate regarding the physical origin of this variable component, many of the models have adopted a magnetic mechanism in which the infrared variability is due to synchrotron emission from a temporarily accelerated population of electrons and the X-ray emission is either a continuation of this synchrotron emission or synchrotron self-Comptonized emission from the same electron population that gives rise to the infrared emission.

The results from this paper support the synchrotron flare models in a number of ways. First, our observations show that, unlike at X-ray wavelengths, the emission at infrared wavelengths appears to have no true steady state component.[9] Our $L' = 14.7$ mag, or dereddened flux density of 1.3 mJy, detection of Sgr A*-IR is a factor of 3 fainter than any previous detection. So while temporarily stable flux densities (the so-called interim quiescent values) have been reported by Genzel et al. (2003a) and Eckart et al. (2004), there appears to be no long-term true steady state at infrared wavelengths. Here it is worth adding a cautionary note regarding the results that are derived from aperture photometry; in such a crowded field apparent steady states can easily be created from stellar confusion, the level of which will change on roughly month timescales due to the motions of stars as they undergo periapse passage. If the flares are caused by magnetic field reconnection or some other local heating event that generates a highly accelerated electron population, there is no predicted steady state component.

A second source of support for synchrotron flare models from this work is the observed infrared colors, which are predicted and observed to be red. However, it is interesting to note that the infrared color reported here and by Eisenhauer et al. (2005), while both red, are significantly different from each other. Our observed $K' - L'$ color of 3.0 ± 0.2 corresponds to a dereddened value of 1.4 ± 0.2, which if modeled as a power law ($F_\nu \propto \nu^\alpha$) gives $\alpha = -0.5 \pm 0.3$. As shown in Figure 5, this is substantially bluer than the spectral index obtained by Eisenhauer, $\alpha \sim -4 \pm 1$, from spectral observations between 2.0 and 2.4 μm. While these spectral indices are inferred from different types of measurements, it is difficult to invoke a calibration error, such as improper rereddening or data extraction, or the 1 minute time lag in our observations, that is large enough to account for the discrepant spectral indices. It is, however, straightforward to invoke plausible physical differences. A spectral break between 2.4 and 3.8 μm could account for the different inferred spectral indices. Such a spectral break is necessary to invoke between the Eisenhauer measurement and the dereddened mid-infrared limits from Sgr A* reported by Morris et al. (2001; 50 mJy at 12.5 μm, 70 mJy at 20.8 μm, and 85 mJy at 24.5 μm), since a constant power law extrapolated from our lowest L' measurement would imply extremely large mid-infrared fluxes (150–2300 mJy). However, this is not necessary for our values, which predict mid-infrared fluxes of only $\sim$2–3 mJy, well below the current mid-infrared limits, from extrapolations of our lowest L' measurement. Furthermore, while such large spectral breaks might be reasonable to invoke between near-infrared and mid-infrared wavelengths, they are rather difficult to invoke over the small wavelength difference between our ex-
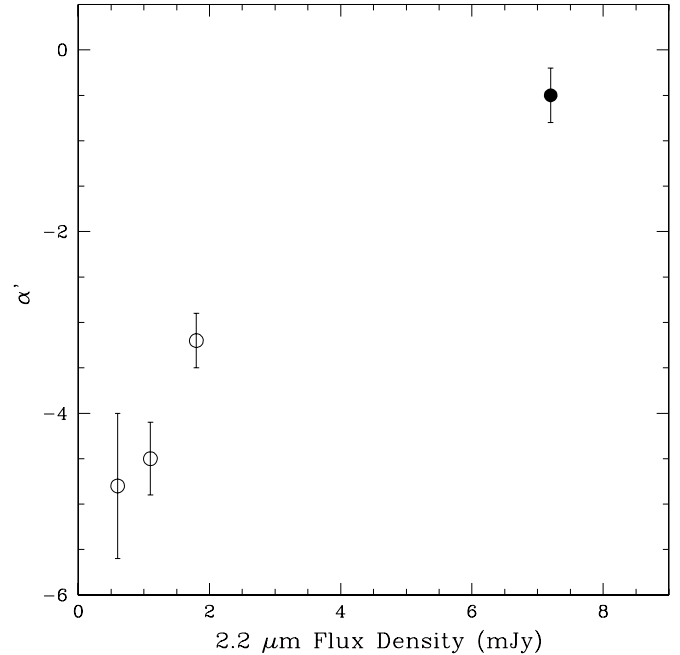

Fig. 5.—Sgr A*'s infrared spectral index (α, where $F_\nu \sim \nu^\alpha$) as a function of its 2 μm flux density. Our measurement is the filled circle, and measurements from Eisenhauer et al. (2005) are the open circles. We suggest that the spectral index may depend on the strength of Sgr A*'s infrared brightness.

periment and that of Eisenhauer et al. (2005). More intriguingly, as an explanation, the spectral index derived by this work was obtained from measurements taken when Sgr A*-IR was a factor of $\sim$6 brighter than it was during the Eisenhauer measurements (see Fig. 5). Thus, a possible cause for the discrepancy may be an infrared spectral index that depends on the strength of Sgr A*-IR's emission. Such a dependence could suggest that events that generate a higher fraction of energetic electrons are responsible the stronger infrared flares.

7. SUMMARY

We have obtained the first observations of the Galactic center with a Laser Guide Star Adaptive Optics system, demonstrating the power of this technique. It has produced the sharpest L' (3.8 μm) images yet of this region. Furthermore, compared to Keck's NGSAO performance on the Galactic center, LGSAO results in L' Strehl ratios that are a factor of 2 higher and a factor of 4–5 more stable. This imaging performance enhancement has permitted us to clearly image an extended infrared emission feature located a mere 90 mas from the central black hole. This object is likely to be a relatively hot dust feature that is locally heated by an embedded or nearby star and that is projected along the line of sight toward Sgr A*. In addition, with improved image quality, Sgr A* can be reliably detected in much shorter time exposures, which has permitted a measurement of Sgr A*'s infrared color. In our measurement, Sgr A* is much bluer and brighter than was measured by Eisenhauer et al. (2005). Among the many possible interpretations for this discrepancy, one intriguing possibility is that Sgr A*'s infrared spectral index is variable and that events leading to stronger infrared flares generate a higher fraction of energetic electrons. In conclusion, LGSAO has improved the quality and versatility with which diffraction-limited observations can be made at the Keck telescope and is ushering in an exciting new era of observations of the Galactic center.

[9] It should be noted that the X-ray steady state component is spatially resolved with a size that corresponds to the Bondi radius ($\sim$1″) and thus comes from scales much larger than those being probed at infrared wavelengths.

REFERENCES

Baganoff, F. K., et al. 2001, Nature, 413, 45

Blum, R. D., Sellgren, K., & DePoy, D. L. 1996, ApJ, 470, 864

Clénet, Y., Rouan, D., Gratadour, D., Marco, O., Léna, P., Ageorges, N., & Gendron, E. 2005, A&A, 439, L9

Diolaiti, E., Bendinelli, O., Bonaccini, D., Close, L., Currie, D., & Parmeggiani, G. 2000, A&AS, 147, 335

Eckart, A., & Genzel, R. 1997, MNRAS, 284, 576

Eckart, A., Genzel, R., Ott, T., & Schödel, R. 2002, MNRAS, 331, 917

Eckart, A., et al 2004, A&A, 427, 1

Eisenhauer, F., Schödel, R., Genzel, R., Ott, T., Tecza, M., Abuter, R., Eckart, A., & Alexander, T. 2003, ApJ, 597, L121

Eisenhauer, F., et al. 2005, ApJ, submitted (astro-ph/0502129)

Genzel, R., Pichon, C., Eckart, A., Gerhard, O. E., & Ott, T. 2000, MNRAS, 317, 348

Genzel, R., Schödel, R., Ott, T., Eckart, A., Alexander, T., Lacombe, F., Rouan, D., & Aschenbach, B. 2003a, Nature, 425, 934

Genzel, R., et al. 2003b, ApJ, 594, 812

Ghez, A. M., Klein, B. C., Morris, M., & Becklin, E. E. 1998, ApJ, 509, 678

Ghez, A. M., Morris, M., Becklin, E. E., Tanner, A., & Kremenek, T. 2000, Nature, 407, 349

Ghez, A. M., Salim, S., Hornstein, S. D., Tanner, A., Lu, J., Morris, M., Becklin, E. E., & Duchêne, G. 2005, ApJ, 620, 744

Ghez, A. M., et al. 2003, ApJ, 586, L127

———. 2004a, AAS Meeting, 205, 24.06

———. 2004b, ApJ, 601, L159

Goldwurm, A., Brion, E., Goldoni, P., Ferrando, P., Daigne, F., Dechourchelle, A., Warwick, R. S., & Predehl, P. 2003, ApJ, 584, 751

Hardy, J. W. 1998, Adaptive Optics for Astronomical Telescopes (New York: Oxford Univ. Press)

Melia, F., & Falcke, H. 2001, ARA&A, 39, 309

Moneti, A., Stolovy, S., Blommaert, J. A. D. L., Figer, D. F., & Najarro, F. 2001, A&A, 366, 106

Morris, M., Tanner, A. M., Ghez, A. M., Becklin, E. E., Cotera, A., Werner, M. W., & Ressler, M. E. 2001, BAAS, 33, 841

Nayakshin, S., Cuadra, J., & Sunyaev, R. 2004, A&A, 413, 173

Porquet, D., Predehl, P., Aschenback, B., Grosso, N., Goldwurm, A., Goldoni, P., Warwick, R. S., & Decourchelle, A. 2005, A&A, 430, L9

Schödel, R., Ott, T., Genzel, R., Eckart, A., Mouawad, N., & Alexander, T. 2003, ApJ, 596, 1015

Schödel, R., et al. 2002, Nature, 419, 694

Stolovy, S. R., Hayward, T. L., & Herter, T. 1996, ApJ, 470, L45

Tokunaga, A. T. 2000, in Allen's Astrophysical Quantities, ed. A. N. Cox (New York: Springer), 150